Active Contour Model

Related terms:

Image Segmentation, Image Processing, Segmentation, Active Contour, Deformable Model, Energy Functionals, Gradient Vector, Initial Contour

View all Topics

Advanced Video Coding: Principles and Techniques

King N. Ngan, ... Douglas Chai, in Advances in Image Communication, 1999

Definition and Properties

An active contour model or more commonly known as *snake* is an energy minimizing spline guided by external constraint forces and influenced by image forces that pull it toward features such as lines and edges. The name arises from the behaviour that is similar to that of a snake, that is, it locks onto nearby edges and localizes them accurately.

A contour can be represented by a vector $v(s) = [x(s), y(s)]$, having the arc length s. With this definition, the energy functional of the active contour model is defined as

(4.6)

where $E_{internal}$ represents the internal energy of the contour due to bending or discontinuities, E_{image} is the image forces, and $E_{constraint}$ is the external energy due to other factors. The extracted contour corresponds to local minima of the energy functional.

> Read full chapter

Motion Artifacts Compensation in DCE-MRI Framework Using Active Contour Model

R. Setola, ... B.B. Zobel, in Emerging Trends in Applications and Infrastructures for Computational Biology, Bioinformatics, and Systems Biology, 2016

27.3 Active Contour

Active contour models (or snakes), introduced in [8] are deformable contours that have been used in many image analysis applications, including the image-based tracking of rigid and nonrigid objects, they represent a special case of the general multidimensional deformable model theory [9].

In their basic forms, the mathematical formulation draws from the theory of optimal approximation involving a functional. A traditional snake is a parametric contour embedded in the image plane . The contour is represented as a parametric curve:

(8)

where $X(s)$ and $Y(s)$ are the coordinate functions and is the parametric domain. This curve is generally obtained using B-splines functions [5,6,10,11] that allow one to depict a continuous and smoothing parameterized contour. B-splines are a particular, computationally convenient representation for spline functions. In the B-spline form, a spline function $V(s)$ is constructed as a weighted sum of NB basis functions (hence, B-splines) ; where, in the simplest (regular) case, each basis function consists of d polynomials each defined over a span of the *s-axis*, having unit length. The basic idea of the B-splines is that it is possible to obtain a contour as a combination of a set of curve as a replication of a basis function. For each basis function, $Bj(s)$, a control point must be defined and the curve is a weighted vector sum of those control points, written as follows:

(9)

where $Bj(s)$ is the polynomial basis function, s is the curve parameter, and is a point in the 2-D image. In the presented approach, we use a simple quadratic B-spline. The first B-spline basis function $B_0(s)$ has the following form:

(10)

and the rest are mere translated copies of the first one.

One may rewrite the sum in Eq. (9), taking into account that active contours are closed lines and by using the arithmetic modular, as follows:

(11)

By varying the number and the location of the control points it is possible to change the contour smoothness and its ability to fit a generic figure.

It is possible to associate to each Active Contour (AC) an energy function [8,12–14,20-], which represents a measurement:

(12)

where the first term is the internal energy and the second one expresses the external energy at the *i*th position of the contour. The internal energy is used to control the rate of stretch and to prevent discontinuity in the contour and can be defined as follows:

(13)

where and are weighting parameters that control the snake's tension and rigidity, respectively. The first term in Eq. (13) is related to the contour elasticity, while the second term specifies the contour's strength and resistance against sudden changes.

The second term in Eq. (12) represents the external energy, which moves a snake to the feature of interest (eg, borders) in an image. This value will be minimal when the snake arrives at the features of interest. It can be defined as follows:

(14)

(15)

where $I(x, y)$ is a gray-level image and $G(x, y)$ is a Gaussian function.

The filter effects are to make a surface uniform, eliminating spikes and ripples due to noise and to blur the image, whereas the gradient effect is to find out the edge of the image and make the external energy responsible for the attractive action toward the edges themselves [8,13].

The contour and its energy function depend only on the *NB* control points location; hence, the problem is to find the best contour that approximates the edge of the ROI. From a mathematical point of view, this can be reduced to the minimization of the energy function (Eq. 12). The optimum location of the snake are searched so that the snake energy can be minimized. A snake that minimizes E_{snake} satisfies the Euler equation. With respect to Eqs. (12)–(14) one obtains

(16)

(17)

The previous equations do not admit a closed-form solution. Numerical techniques, such as gradient descend method (GDM), provide a method for unconstrained minimization based on the use of search direction opposite to the gradient. A physical interpretation of Euler equations can be viewed as a force balance equation that drives the snake toward the minimum contribution of the corresponding energy by changing the coordinates of the contour according to the images characteristics.

(18)

Each term of Eqs. (16), (17) is the combination of two different types of forces, internal and external, whose contributions is properly weighted by the parameters □, □, *k*. The internal forces can be classified as elastic and bending forces that prevent the contour from stretching and bending while the external force plays an attractive action toward the edge of the ROI. Applying the GDM, one obtains the following iterative equations, which are the discrete version of Eqs. (16), (17):

(19)

(20)

where and collect the coordinates of the new contour while *Xk* and *Yk* collect the same quantity for the current one; *k* is the iteration index and Δ is the algorithm step. Eqs. (19), (20) produce a sequence of contour point locations that minimize more and more the energy of the snake; the process is generally stopped when the next iteration does not introduce a significant change of the total energy (Eq. 12). The crucial point to guarantee the rapid convergence of the iterative equations is the need to adopt as initial contour points (ie, X_0, Y_0) belonging to a region sufficiently close to the actual contour.

> Read full chapter

Introduction to Medical Image Recognition, Segmentation, and Parsing

S.Kevin Zhou, in Medical Image Recognition, Segmentation and Parsing, 2016

1.6.2 Active Contour Method

The active contour model or snake (Kass et al., 1988) seeks a parameterized curve that minimizes the cost function :

(1.17)

where μ controls the magnitude of the potential, ∇ is the gradient operator, $\mathbf{I}$ is the image, $w_1(s)$ controls the tension of the curve, and $w_2(s)$ controls the rigidity of the curve. The implicit assumption of the snake model is that edge defines the curve due to the use of the gradient operator. The gradient descent minimization computes the force on the snake, defined as the negative of the gradient of the energy field, which evolves the curve. Important variants of the active contour model include the gradient vector flow snake model (Xu and Prince, 1998), geodesic active contour (Caselles et al., 1997), etc.

> Read full chapter

Processing, Analyzing and Learning of Images, Shapes, and Forms: Part 2

Da Chen, Laurent D. Cohen, in Handbook of Numerical Analysis, 2019

1 Introduction

The original active contour model proposed by Kass et al. (1988) is a variational approach for the applications of boundary detection, image segmentation and object tracking. It is capable of locally minimizing an energy functional for the purpose of detecting an optimal and continuous curve, either open or closed, to depict the image features of interest such as image edges. The energy functional of this model can be established using the image grey levels or gradients. A broad variety of region-based active contour approaches have been intensively studied in order to develop the original active contour model (Kass et al., 1988). They take into account a type of more robust regional homogeneity penalization way for image segmentation. As a consequence, these region-based variant approaches are able to search for suitable solutions in more complicated situations. In the other hand, the minimal geodesic path model was first introduced by Cohen and Kimmel (1997) in order to search for the global minimum of a simplified version of the functional used in the original active contour model (Kass et al., 1988). In essence, this simplified active contour energy functional can be regarded as a weighted curve length and it can be solved through the Eikonal partial differential equation (PDE). The objective of this chapter is to show how the terms that are commonly used in the active contour models can be handled using different kinds of metrics for geodesic paths, in particular Randers metrics.

In its basic formulation, the minimal geodesic path model extracts image features by a globally optimal curve between two prescribed points, usually provided by the user. A minimal path can be tracked through the solution to the Eikonal PDE. A large num-

ber of well-established Eikonal solvers have been exploited such as the fast marching methods (Mirebeau, 2014a, b, 2018; Sethian, 1999). The global optimality and the efficient solutions lead to a series of successful minimal path-based applications as reviewed in Peyré et al. (2010). However, the original minimal geodesic path model (Cohen and Kimmel, 1997) depends only on the first-order derivative term of a curve. Thus this model cannot impose curvature to define the regularization term which corresponds to the curve rigidity property. Finally, in the minimal path-based image segmentation scenario, almost all of the existing geodesic metrics (Appia and Yezzi, 2011; Benmansour and Cohen, 2009; Mille et al., 2015) are derived from the image boundary features, which may limit their performance on complicated image segmentation tasks. In the remaining of this chapter, we proposed different geodesic metrics to overcome the aforementioned drawbacks suffered by the existing minimal path models.

In Kimmel (2003) and Kimmel and Bruckstein (2003), the authors proposed a listing of the active contour energy terms for image segmentation. In our chapter, we propose to revisit Kimmel's chapter (Kimmel, 2003), named *fast edge integration*, with minimal path methods to address the active contour problems.

1.1 Outline

In this chapter, we illustrate different types of geodesic metrics and their respective applications in image analysis based on the minimal path framework and the Eikonal PDE. The structure of this chapter is organized as follows:

- In Section 2, we present the preliminary background on the active contour models involving the approaches, respectively, driven by edge- and region-based terms.
- In Section 3, we review the existing minimal path models associated with both of the Riemannian and Randers metrics, the corresponding Eikonal PDEs for the computation of the geodesic distance as well as the gradient descent ordinary differential equations (ODEs) for tracking geodesic curves.
- In Section 4, we present two minimal path models for the minimization of the geometric active contour models with alignment terms (Kimmel, 2003; Kimmel and Bruckstein, 2003). We, respectively, induce a Randers metric and an anisotropic Riemannian metric from the variants of the asymmetric and symmetric alignment terms. In this case, the active contour problems with different alignment terms are transferred to the corresponding minimal path problems.
- In Section 5, we present a Finsler elastica minimal path model (Chen et al., 2017) to solve the Mumford–Euler elastica curve problem (Mumford, 1994). This is done by using a strongly anisotropic and asymmetric Randers geodesic metric that is established over an orientation-lifted space. The orientation

dimension is used to represent the curve directions. The introduced Finsler elastica minimal paths can be naturally applied for the applications of retinal imaging and boundary detection.

- In Section 6, we present a new method that applies the Randers minimal path model to address the region-based active contour problems (Chen et al., 2016, 2019). The used Randers metric is derived from the region-based homogeneity term as well as the curve length-based regularization term, relying on the solution to divergence equation-constrained minimization problem. In this case, we can make use of the Randers Eikonal PDE to solve a broad variety of region-based active contour problems.

> Read full chapter

Specialized Neural Networks Relevant to Bioimaging

Anke Meyer-Baese, Volker Schmid, in Pattern Recognition and Signal Analysis in Medical Imaging (Second Edition), 2014

10.8.1 Mathematical Model of the Active Contour

The basic active contour model is an energy-minimizing spline. For any point of the contour, an energy function can be defined as [169]

(10.24)

The first two terms describe the internal energy of the contour, while the final term refers to the image forces. The first- and second-order derivatives of are approximated as follows:

(10.25)

and

(10.26)

and are the - and -coordinates of the th boundary point . In [408], the contour has to be attracted to edge points, and therefore the image forces depend on the gradient of the image at point

(10.27)

The basic idea proposed in [408] is that the boundary is detected by iteratively deforming an initial approximation of the boundary through minimizing the following energy functional:

(10.28)

Before employing the active contour model, an initial contour must be estimated. In

[408]

, the contour for the first slice is estimated based on morphological operations.

> Read full chapter

Geometric Active Contours for Image Segmentation

Vicent Caselles, ... Guillermo Sapiro, in Handbook of Image and Video Processing (Second Edition), 2005

3.1 Geodesic Active Contour

The geodesic active contour model [10] is defined by the functional

It is an integration of an inverse edge indicator function, [i.e. any decreasing function of the modulus of the gradient, such as $g(x,y) = 1/(1 + |\nabla I|^2)$], along the contour. The search, in this case, is for a curve along which the inverse edge indicator gets the smallest possible values. This curve is a geodesic. That is, we would like to find the curve C that minimizes this functional. Modifying the function g, different results can be obtained. For example, segmentation of vector valued images [45, 64] or even solving the 3D from stereo problem [26]. This geometric energy, up to an arbitrary constant, can be obtained by manipulating the classic snakes [37] using least-action principles in physics (see also Aubert and Blanc-Feraud [2]). In addition to its use for fundamental image-processing problems, the geodesic active contour can serve as a regularization term for other variational-based segmentation formulations [41]. We point out that a well-studied example of this functional is $g = 1$, for which the functional measures the total arc-length of the curve.

> Read full chapter

Processing, Analyzing and Learning of Images, Shapes, and Forms: Part 2

Christos Sakaridis, ... Petros Maragos, in Handbook of Numerical Analysis, 2019

1 Introduction

Evolution of curves via active contour models has been applied extensively in computer vision for image segmentation. In the standard image setting which involves a regular grid of pixels, the discretization of partial differential equations (PDEs) governing the motion of active contours is well-established (Osher and Sethian, 1988) and ensures proper convergence of the contour to object boundaries. Recently, active contour models based on level set PDE formulations have been extended (Drakopoulos and Maragos, 2012; Kolotouros and Maragos, 2017; Sakaridis et al., 2017) to handle more general inputs in the form of graphs whose vertices are arbitrarily distributed in a two-dimensional Euclidean space. In particular, the input in this case consists of:

1. an undirected graph , where and , and
2. a real-valued function defined on the vertices of the graph, which resembles the image function in the standard grid setting. For the rest of the paper, we will use the term image function to refer to I.

Applications of segmentation of such graphs span not only image processing but also geographical information systems and generally any field where data can assume the form of a set of pointwise samples of a real-valued function. The arbitrary spatial structure of these graphs poses a significant challenge to the discretization of active contour PDEs.

This chapter presents two fundamentally distinct approaches that have been developed to accomplish the aforementioned discretization. The first approach, which is introduced in Drakopoulos and Maragos (2012) and Sakaridis et al. (2017), takes a *finite difference* path and proposes geometric approximations of the continuous differential operators that are involved in active contour PDEs, namely *gradient* and *curvature*, on graphs with arbitrary vertex and edge configuration. The second approach, which is proposed in Kolotouros and Maragos (2017), leverages *finite elements* to approximate the solution of these PDEs on graphs with arbitrary vertex configuration that constitute a triangulation. Both approaches have been used in Sakaridis et al. (2017) and Kolotouros and Maragos (2017) to successfully apply the widely used models of geodesic active contours (GACs) (Caselles et al., 1997) and active contours without edges (ACWE) (Chan and Vese, 2001) to arbitrary 2D graphs for graph and image segmentation.

The chapter is structured as follows. Section 2 reviews related work on active contours, graph-based morphology and segmentation, and PDE-based methods on graphs, and provides the necessary background on the employed active contour models. Section 3 outlines the finite difference approach of Sakaridis et al. (2017) for active contours on graphs. It is composed of Section 3.1 on the geometric gradient approximation on arbitrary graphs and its asymptotic consistency and accuracy in the limit of infinite vertices for the class of random geometric graphs (Penrose, 2003), Section 3.2 on the geometric curvature approximation and its convergence in probability, and Section 3.3 on improved Gaussian smoothing on graphs for initialization of the GAC model through normalization. Section 4 outlines the finite element approach of Kolotouros and Maragos (2017). More specifically, Section 4.1 discusses the problem formulation and analyzes the key aspects of the finite element approximation for active contour models. Section 4.2 presents an extension of the previous framework for locally constrained active contour models that can additionally be used for speeding up contour evolution. Last, Section 5 presents experimental results of the two approaches on segmentation from the translation of GACs (Caselles et al., 1997) and ACWE (Chan and Vese, 2001) to arbitrary graphs created from regular images or containing geographical data and Section 6 recapitulates the main components of the chapter and provides a discussion on future research directions.

> Read full chapter

Polyp Segmentation on CT Colonography

J. Yao, R.M. Summers, in Medical Image Recognition, Segmentation and Parsing, 2016

20.4.3.4 Adaptive deformable models

After the image is enhanced and potential fold regions are marked, an adaptive deformable model is applied on the membership map to locate the polyp boundaries. Deformable models have been widely used in medical image segmentation (McInerney and Terzopoulos, 1996). The active contour model is the most commonly used model in 2D image segmentation, which was first introduced by Kass et al. (1988).Cohen (1991) proposed a balloon force that significantly increases the capture range. The active contour model was later extended to 3D images (Cohen and Cohen, 1993; Xu et al., 2000). Here, in this method, the traditional deformable model is enhanced by introducing a counter-force to control the model evolution

on the haustral fold and by adaptively maintaining the model resolution during the evolution.

An initial model of the polyp is first placed at the seed location and the initial parameters are set. Then an iterative process is started. During each iteration, deformation forces are computed, and the model is updated according to the forces. Then the force weights and other control parameters are adaptively updated. The model resolution and topology is also adaptively maintained. The iterative process is repeated until all forces reach a balance (the model remains unchanged during two iterations) or a maximum number of iterations (currently 100, which exceeds the maximum polyp size) are executed.

The deformable model is represented as triangular meshes. The mesh data structure consists of a list of triangles and a list of vertices. Each vertex stores its 3D coordinate and a set of reference pointers to incident triangles. Each triangle stores reference pointers to its vertices and reference pointers to adjacent triangles sharing common edges. The so-called winged data structure was first introduced in Baumgart (1975), which allows efficient retrieval of vertex neighbors and triangle neighbors.

The initial model is a $2 \times 2 \times 2$ cube at the seed point. The deformable model is driven by the combination of internal force, image force, external force, and a counter-force in the fold region. The internal forces intend to maintain the smoothness and continuity of the model. They are computed as

(20.8)

where s is the surface model and v is a vertex on the model. The first term on the right-hand side is the first-order partial derivative which makes the model continuous and acts like an elastic membrane. The second term is the second-order derivative which makes the model smooth and acts like a rigid thin plate. By adjusting the weights $\square$ and $\square$, the relative importance of the membrane term and the thin-plate term is balanced.$\square = 1$ and $\square = 1$ are used in the method.v is the 3D coordinate of a vertex. $\square_2$ is the partial derivatives which are computed using a Laplacian operator and finite difference on the triangular mesh.

Polyp boundaries tend to have larger gradients than other regions on the membership map. Therefore, the gradient of the edge map can be used as the image forces to attract the model, that is

(20.9)

where $\mu(v)$ is the membership map of "polyp tissue" class, $\square$ is the gradient operator, and $G\square$ is the Gaussian operator, which is used to smooth the image and increase the capture range. computes the gradient magnitude of the membership map, which represents an edge map.

An expansion force is exerted to inflate the model from its initial state and prevent it from collapsing. The expansion force at a vertex v is

(20.10)

where $N(v)$ is the surface normal at vertex v. The expansion force points outward in the direction of surface normal.

Polyps on haustral folds need special treatment since the deformable model often leaks into the fold region.Figure 20.10(f) shows an over-segmented polyp on the fold. In order to address this problem, one more force is introduced in the deformable model to offset the expansion force at the fold region. The so-called counter-force is written as

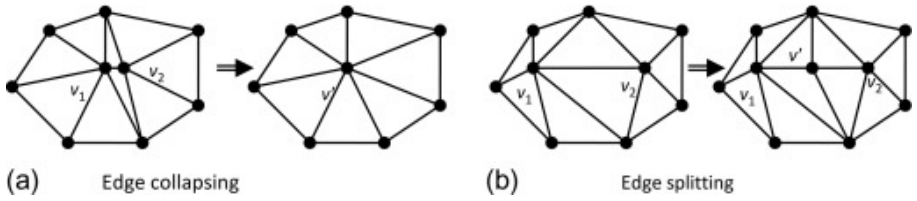

Figure 20.9. Adaptive model maintenance operations.

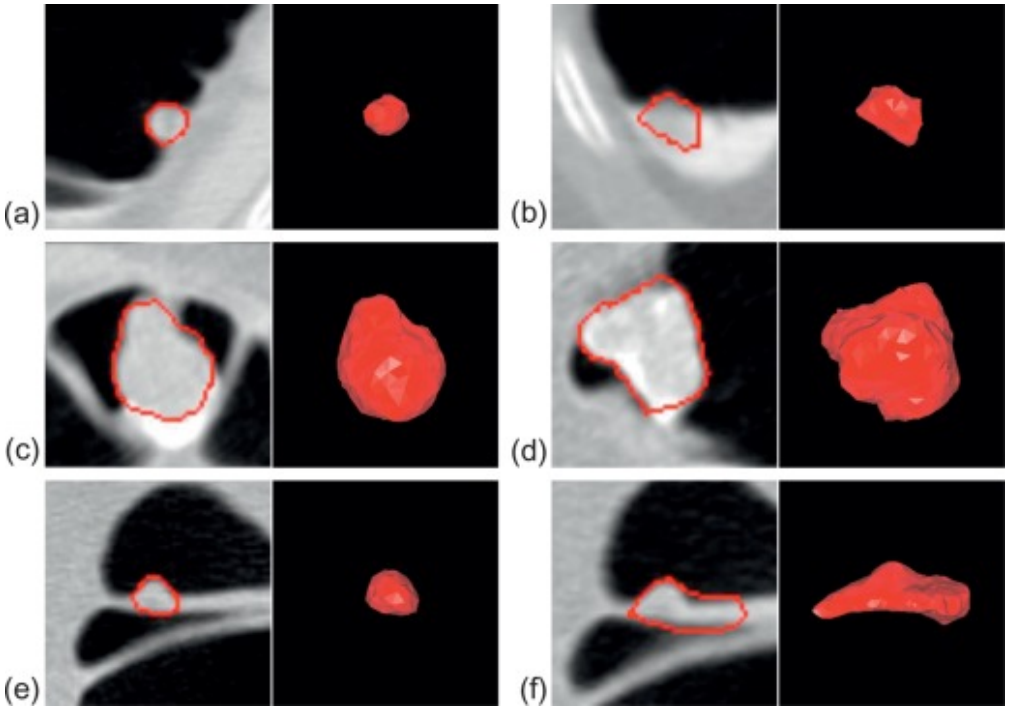

Figure 20.10. Segmentation results: left of each pair is 2D axial images superimposed with segmentation result; right of each pair is 3D surface reconstruction of the segmentation. (a) 7 mm sessile polyp; (b) 11 mm polyp under fluid; (c) 20 mm lobulated mass; (d) 20 mm lobulated mass; (e) segmentation of a 10 mm polyp on-fold with counter-forces; (f) segmentation of same polyp without counter-forces.

(20.11)

After adding the counter-force, the force equation in the deformable model becomes:

(20.12)

where $w_{counter} = w_{expansion}.w_{expansion} = 5$, $w_{internal} = 2$, and $w_{image} = 5$ are set empirically in the current method. $\vec{n}(v)$ is the normal direction at v. The location of a vertex v on the model is updated at each iteration using Eq. (20.12),

(20.13)

where t is the evolution time, Δ is the step size, and F is the deformation force.

The model resolution is measured by the distance between adjacent vertices (i.e., the edge length). It is desirable to maintain the resolution during the model evolution. If the resolution is too high (vertices are too close), too many vertices need to be updated during each iteration which therefore slows down the converging process. On the other hand, if the resolution is too low (vertices are too sparse), there might not be a sufficient number of vertices to accurately snap the boundary. Furthermore, uneven vertex distribution will cause uneven internal and expansion forces, which may result in incorrect model deformation. Therefore, evenly distributed vertices are also desirable, that is, the resolution should be consistent throughout the model.

Two edge-based operations are carried out to adaptively maintain the model resolution: (1) if one edge is too short, it will be collapsed into one vertex; (2) if one edge is too long, it will be split into two edges by inserting one vertex in the middle. After each operation, the neighborhood will be retiled to form a valid triangular mesh.Figure 20.9 illustrates the adaptive mesh maintenance operations. In Figure 20.9(a), edge $v_1 - v_2$ is collapsed into one vertex v_0 and its neighborhood is retriangulated. In Figure 20.9(b), edge $v_1 - v_2$ is split into two edges by inserting a vertex v_0, and the two triangles incident to the edge are also split into four triangles. The edge length is maintained at the length of 1-4 voxel size in the current method.

Figure 20.10(a) shows the visual results of some segmented polyps with and without the counter-force. The examples include a medium-sized sessile polyp (Figure 20.10(b)), a polyp under fluid (Figure 20.10(c)), two lobulated masses (Figure 20.10(e) and (d)), and polyps on haustral folds (Figure 20.10 and (f)) (Yao and Summers, 2007). The visual results showed that the deformable model produced generally accurate polyp-lumen border and a fairly good estimate for the polyp-colon borders. The segmentation running time is less than 3 s for most polyps.

> Read full chapter

Image Analysis for Medical Visualization

Bernhard Preim, Charl Botha, in Visual Computing for Medicine (Second Edition), 2014

4.5.1 Active Contour Models

Deformable models are based on a flexible geometric representation, such as B-splines, which provide the necessary degrees of freedom to adapt the model to a large variety of shapes. The process of fitting the model to the target structure is guided by physical principles and constraints which restrict, for example, the curvature along the boundary and thus favors smooth boundaries. The application of deformable models is guided by principles of elasticity theory, which describe how deformable bodies respond to forces. The resulting shape variations depend on some assumed stiffness properties of that body. Deformable models for image segmentation were suggested by Terzopoulos *et al.* [1988].

Active contour models or *snakes*—as they are often called—are a variant of deformable models, where initial contours are algorithmically deformed towards edges in the image [Kass *et al.*, 1988]. They are primarily used to approximate the shape of smooth object boundaries. The name *snake* is motivated by the behavior of such models, which adapt a contour between two control points like a snake.

The initial contour is either supplied by the user or derived from a priori knowledge (concerning geometric constraints, object shapes, and data constraints, such as range of expected gray level). Starting from the initial contour, an *energy functional* is minimized, based on contour deformation and external image forces. This optimization process cannot guarantee that a global minimum is found. Instead, a local minimum—based on the initial contour—is accepted.

Internal and External Energies The energy function with a parametric description of the curve , where and represent the coordinates along the curve is described by Equation 4.12

(4.12)

The inner energy (Eq. 4.13) represents the smoothness of the curve and can be flexibly parameterized by and to encode expectations concerning the smoothness and elasticity of the target structure's contour. High values, for example, contract the curve. Usually, and are constant [Lehmann *et al.*, 2003].

(4.13)

The external energy counteracts the inner energy and is derived by the gray values and the gradient of the image according to Equation 4.14:

(4.14)

and are weights, which represent the influence of the gray value and the gradient . The gray values are assumed to be normally distributed with the standard deviation .

The curves are usually represented as (cubic) B-splines, which has the advantage that the resulting segmentation is smooth (continuous first order derivatives). The actual realization of the functional is very application-specific.

Balloon Segmentation as 3D Extension For 3D segmentation, active contour models are applied slice by slice, which is not only laborious, but also poses problems in the composition of a continuous surface based on a stack of contours. To better support 3D segmentation, the fitted contour in one slice may be used as initial contour in neighboring slices [Lin and Chen, 1989]. This process of *contour propagation* can be applied in a similar way than in livewire segmentation (recall § 4.4.1). Also, a combination with shape-based interpolation is feasible.

Active contour models have been extended to 3D, which is known as *balloon segmentation* [Terzopoulos *et al.*, 1988]. Balloon segmentation is based on deforming surfaces instead of contours. This is accomplished by interactively fitting a polygonal representation of the initial shape to the target structure. There are two approaches how the segmentation process is initiated: either the user selects small volumes that are iteratively inflated until the forces converge, or enclosing volumes are specified by the user and iteratively deflated. Figure 4.23 illustrates the inflation with an application to tumor segmentation.

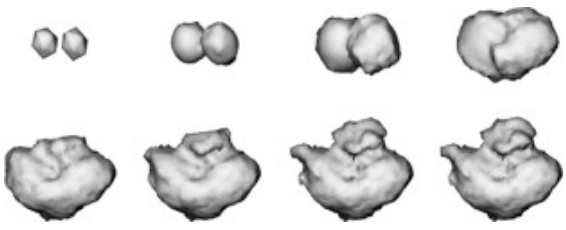

Figure 4.23. Inflating balloon segmentation starting from the two small volumes in the upper left. After 40 iterations the final tumor segmentation is achieved (lower right image).

(Courtesy of Olaf Konrad-Verse, Fraunhofer MEVIS Bremen)

These 3D extensions bear a great potential. However, they pose some challenging user-interface problems (3D interaction with 2D input and output devices).

Discussion The internal energy constraints of active contour models restrict their flexibility and prevent that they represent tube-like shapes, branching structures

or objects with strong protrusions [McInerney and Terzopoulos, 1996]. Therefore, they are generally not applied for the segmentation of vascular or bronchial trees. A problem of active contours (and their 3D extensions) is the strong dependence on a proper initialization; the contour might otherwise be attracted by a "wrong" edge in an image. A "wrong" edge is usually a part of the border of a nearby image but can also be an artifact. Although nice results can be presented in many publications, active contour models are (still) not widespread in clinical applications due to their difficult parameterization.

> Read full chapter

Challenges and future directions in neutrosophic set-based medical image analysis

Deepika Koundal, Bhisham Sharma, in Neutrosophic Set in Medical Image Analysis, 2019

4.2.9 Other medical images

In this method, the integration of NS and a multiscale similarity measure is presented for detecting white blood cells (WBCs) in the blood smear images. To determine the similarity among diverse color components of the blood smear image, the NS similarity score is used. The segmentation method is carried out without any morphological operations. At some point in the future, the whole CAD system will be developed for WBC identification and the connected blast cells will be isolated in order to recognize the staining artifacts, accelerate and enhance the projected method as it worked under multi-criteria that consumed more time (Shahin, Amin, et al., 2018; Shahin, Guo, et al., 2018). A neutrosophic active contour model (NACM) has been presented for the detection and segmentation of the myocardium region in the short-axis left ventricle of the myocardial contrast echocardiogram (SLVMCE) image (Guo, Du, et al., 2017). The similarity value in NS has been well defined through homogeneity, which has features to interpret the fuzziness such as low contrast, speckle noise, and a vague boundary on MCE. The myocardium region is lastly found by evolving the curve. The solution defined in the presented NACM technique can find and segment the LVMCE images rapidly and correctly (Guo, Ashour, & Sun, 2017; Guo, Budak, et al., 2017; Guo, Du, et al., 2017; Guo, Jiang, et al., 2017). In another work, an improved neutrosophic graph cut scheme is presented for cervical cancer detection. It is used for the extraction of nuclei and cytoplasmic boundaries of the Pap smear cells. This segmentation system improved

the classification rate of cervical cancer detection with an indeterminacy filter to lower the indeterminacy value of spatial information and the extracted intensity values of the preprocessed cancer cell images (Devi, Sheeba, & Joseph, 2018).

> Read full chapter